frontiers in Materials

ORIGINAL RESEARCH
published: 08 November 2019
doi: 10.3389/fmats.2019.00284

Thermoplastic Starch Composites Filled With Isometric and Elongated TiO_2-Based Nanoparticles

Aleksandra Ujcic, Martina Nevoralova, Jiri Dybal, Alexander Zhigunov, Jana Kredatusova, Sabina Krejcikova, Ivan Fortelny and Miroslav Slouf*

Department of Polymer Morphology, Institute of Macromolecular Chemistry, Academy of Sciences of the Czech Republic, Prague, Czechia

Biodegradable thermoplastic starch (TPS) composites with isometric titanium dioxide nanoparticles (TiO_2; diameter ∼100 nm) and elongated titanate nanotubes (TiNT; diameter ∼20 nm and aspect ratio >50) were prepared from wheat and tapioca starch. The preparation was based on our recently developed two-step procedure consisting of the solution casting (SC) followed by the melt mixing (MM), which had been shown to yield highly homogeneous TPS in our previous study. In this work we demonstrated that the type of the TPS matrix and the type of the filler had significant impact on the morphology and the properties of the final composites. Multiple microscopic techniques (LM, SEM, and TEM) evidenced that the TPS/TiO_2 composites exhibited a very homogeneous dispersion of the filler, while the TPS/TiNT composites contained micrometer-size agglomerates of TiNT. Moreover, all composites with the wheat starch matrix [TPS(w)] showed a higher filler agglomeration than the corresponding composites with the tapioca starch matrix [TPS(t)]. Rheological experiments showed that the TiO_2 and TiNT fillers had quite small impact on the viscosity of the TPS(w) matrix, probably due to slightly higher agglomeration, poorer dispersion, and weaker matrix-particle interactions. On the other hand, the TPS(t) matrix was influenced by both fillers significantly: the TiO_2 nanoparticles with almost ideal dispersion formed a physical network in the TPS(t) matrix, which significantly increased the viscosity of the composite, whereas the TiNT nanotubes seemed to destruct the TPS(t) matrix partially, resulting in decreased viscosity of the composite. DMTA results confirmed the rheological measurements: Storage moduli (*G'*) showed that TPS(t) and its composites with TiO_2 were stiffer than the corresponding TPS(w) samples, while the TPS(t)/TiNT composites were less stiff than TPS(w)/TiNT. Also loss moduli (*G"*) confirmed the difference between tapioca starch and wheat starch composites, which differed by their glass transition temperatures [T_g of TPS(w) < T_g of TPS(t)]. The rheological and DMTA results were supplemented and supported by IR, XRD, and TGA measurements.

Keywords: wheat thermoplastic starch, tapioca thermoplastic starch, TiO_2, TiNT, morphology, thermomechanical properties, rheological properties

OPEN ACCESS

Edited by:
Andrea Dorigato, University of Trento, Italy

Reviewed by:
Massimo Messori, University of Modena and Reggio Emilia, Italy
Azman Hassan, University of Technology Malaysia, Malaysia

****Correspondence:***
Aleksandra Ujcic
ostafinska@gmail.com

Specialty section:
This article was submitted to Polymeric and Composite Materials, a section of the journal Frontiers in Materials

Received: *31 July 2019*
Accepted: *22 October 2019*
Published: *08 November 2019*

Citation:
Ujcic A, Nevoralova M, Dybal J, Zhigunov A, Kredatusova J, Krejcikova S, Fortelny I and Slouf M (2019) Thermoplastic Starch Composites Filled With Isometric and Elongated TiO_2-Based Nanoparticles. Front. Mater. 6:284. doi: 10.3389/fmats.2019.00284

INTRODUCTION

Starch is one of the cheapest and the most abundant natural polymers. On this account, starch-based materials are employed in many applications, for example, in household, agriculture, textile, pharmacy, or medicine (Bertolini, 2010; Sarka et al., 2011, 2012; Saiah et al., 2012; Xie et al., 2013; Ghavimi et al., 2015; Campos-Requena et al., 2017; Javanbakht and Namazi, 2017; Kuswandi, 2017; Liu et al., 2017a,b). However, the biggest drawback of native granular starch is processing. The semicrystalline granular starch itself decomposes before melting when processed in classic devices (Biliaderis, 2009). In most applications, the semicrystalline granular starch is transformed into an almost amorphous thermoplastic starch (TPS) matrix by addition of low molecular weight compounds such as water, glycerol, citric acid etc. (Biliaderis, 2009; Bertolini, 2010; Visakh et al., 2012). The starch plasticization is influenced by many factors, mostly: the starch source (wheat, tapioca, corn etc.; Ao and Jane, 2007; Biliaderis, 2009; Bertolini, 2010; Liu et al., 2010), the plasticizer type and amount (Dai et al., 2008; Pushpadass et al., 2008), and the plasticization method and conditions (Altskar et al., 2008; Liu et al., 2013; Xie et al., 2013).

The botanic origin of starch determines the size and shape of starch granules as well as the range of the amylose/amylopectin content (Ao and Jane, 2007; Jane, 2009; Perez et al., 2009; Bertolini, 2010; Liu et al., 2010). In this work we selected two widely used types of starch: wheat starch from the grains of *triticum aestivum* (common wheat) and tapioca starch from the roots of *manihot esculenta* (aka cassava, manioc). Wheat starch has two types of the granules with the sizes ranging from 1 to 45 μm: A-granules (a lenticular shape, large: mean diameter 15 μm) and B-granules (a spherical shape, small: mean diameter 4 μm), and it is normally composed of 75% of amylopectin and 25% of amylose (Maningat et al., 2009). It tends to form an opaque and non-cohesive paste, with a medium resistance to shear and a high retrogradation (Biliaderis, 2009; Bertolini, 2010). Tapioca starch has the granules from 4 to 35 μm which are smooth and irregular spheres, and it is composed of amylopectin containing 17–20% amylose with a higher molecular weight than other types of starch (Breuninger et al., 2009). It forms a transparent and cohesive gel, with a low resistance to shear and a lower retrogradation (Biliaderis, 2009; Bertolini, 2010; Zhu, 2015). As just described, the wheat and tapioca starches vary not only in the size and the shape of their granules, but also in the chemical composition (the amylose/amylopectin ratio; the molecular weight of amylose), which results in the different behavior and properties of final thermoplastic starches.

Many researchers recently studied the properties of wheat thermoplastic starch (Sarka et al., 2011; Kelnar et al., 2013; Mahieu et al., 2015; Schmitt et al., 2015; Song et al., 2018) as well as tapioca thermoplastic starch (Chang et al., 2006; Garcia et al., 2009; Teixeira et al., 2009, 2012; Ajiya et al., 2017; Bergel et al., 2017; Campos et al., 2017, 2018; Gonzalez-Seligra et al., 2017; Guz et al., 2017; Kargarzadeh et al., 2017; Lopez-Cordoba et al., 2017; Genovese et al., 2018; Liu et al., 2018; Valencia-Sullca et al., 2018). It is worth noting that the greatest amount of the thermoplastic starches has been prepared exclusively by a melt mixing (Teixeira et al., 2009, 2012; Sarka et al., 2011; Mahieu et al., 2015; Schmitt et al., 2015; Gonzalez-Seligra et al., 2017; Campos et al., 2018; Genovese et al., 2018; Liu et al., 2018; Song et al., 2018) or exclusively by a solution casting (Chang et al., 2006; Garcia et al., 2009; Kelnar et al., 2013; Ajiya et al., 2017; Bergel et al., 2017; Campos et al., 2017; Guz et al., 2017; Kargarzadeh et al., 2017; Lopez-Cordoba et al., 2017; Valencia-Sullca et al., 2018). Even though the TPS materials prepared by the mentioned single-method procedures were homogeneous at macroscopic level, they still contained non-fully plasticized starch granules and/or inhomogeneities at microscopic level. For example, Teixeira et al. (2012) found some partially destroyed starch granules in cassava TPS prepared by extrusion and Schmitt et al. (2015) found starch granules in continuous phase of wheat TPS prepared by extrusion as well. Gonzalez-Seligra et al. (2017) found that some of cassava TPS's prepared by an extrusion (processed at three different screw speeds) contained broken starch granules. They obtained one TPS with a homogenous surface and two TPS's with the presence of starch granules. Therefore, in our previous paper (Ostafinska et al., 2017) we developed a two-step method of the starch plasticization, consisting of a solution casting (SC), which was followed by a melt-mixing (MM). The two-step SC + MM procedure was shown to be reliable and reproducible method for preparation of homogeneous wheat TPS matrix with well-dispersed TiO_2. Surprisingly, there are not so many studies dealing with TPS/TiO_2 composites. Oleyaei et al. (2016a,b) and Razali et al. (2016) studied similar TPS/TiO_2 systems, but with different types of starches and different plasticization procedures. Moreover, just a few of the publications compared the properties of thermoplastic obtained from different starch sources. For example, Omotoso et al. (2015) studied cassava, corn, potato, and yam TPS prepared by solution casting. Bergel et al. (2017) prepared TPS foams from potato, cassava, and corn starches by solution casting followed by compression molding. Genovese et al. (2018) prepared TPS from wheat, potato, and corn starches by melt-mixing. Song et al. (2018) and Zuo et al. (2017) studied TPS prepared by the solution casting of wheat and corn starch mixture. To the best of authors' knowledge, there are no papers concerning wheat and tapioca thermoplastic starches prepared in the same way, which would compare the properties of both types of TPS that seems to differ significantly.

Due to the above, we focused our attention on the comparison of the systems prepared by our two-step procedure (SC + MM), using two types of starches (wheat and tapioca) and two types of TiO_2-based particles (isometric TiO_2 nanoparticles and high aspect ratio TiNT nanotubes). Titanium-based particles were chosen for our research because they were expected to modify the properties of TPS, while maintaining or even increasing the biocompatibility of the final composites. The TiX-particles were shown to be compatible with both soft tissues and bone cells (Webster et al., 2000; Sengottuvelan et al., 2017). The TPS/TiX composites with tunable properties could be suitable for broader range of medical applications. The morphology, structure, rheology, and thermomechanical properties of wheat and tapioca TPS/TiX composites were studied in order to: (i) verify if SC + MM is the universal method of TPS starch preparation, which yields homogeneous dispersion of filler

regardless of source starch type; (ii) to find possible differences among TPS composites prepared by SC + MM method from different starch types; and (iii) to assess if SC + MM method yields homogeneous dispersion of the filler also at increased concentrations (up to 6 wt.%).

MATERIALS AND METHODS

Materials

Wheat (w; A-granules) and tapioca (t) starches were supplied by Škrobárny Pelhrimov, a.s., Czech Republic. Glycerol anhydrous (G; min. 99%) and sodium bromide (reagent grade) were obtained from Lachner, Czech Republic. Commercial titanium dioxide (TiO_2; anatase, particle size 50–200 nm) was delivered by Sigma-Aldrich, USA. Titanate nanotubes (TiNT) with the low diameter (∼20 nm) and the high aspect ratio (AR = length of the nanotube/diameter of the nanotube >50) were prepared by the hydrothermal synthesis from TiO_2 as described in our previous work (Kralova et al., 2010).

Preparation of TPS/TiX Composites

All samples (**Table 1**) were prepared by our recently developed two-step method: the solution casting (SC) followed by the melt mixing (MM), according to the recipe described in our previous paper (Ostafinska et al., 2017). Briefly, we used SC with a ratio of starch/glycerol = 70/30 (wt.%) and a ratio of starch/water = 1/6 (wt.%) for all samples. In the first step, the TiX particles (TiX = either TiO_2 particles or TiNT nanotubes described above in Section Materials) were dispersed in water using ultrasonic bath for 1 min and then glycerol was added and sonicated for 2 min. The pre-mixed water suspension (starch/glycerol/TiX: 30 min, room temperature) was mixed at the elevated temperature until the viscosity significantly increased (at least 10 min at temperature above 65°C) and then until the mixture became visually homogenous (when temperature increased to 60–70°C for at least 10 min, the starch gelatinized, which resulted in the disruption of the insoluble granules, loss of the molecular organization and an increase in its viscosity Bertolini, 2010). The solution was casted onto thin foils and dried at ambient temperature for 2–3 days, followed by 4 days in a desiccator with saturated solution of sodium bromide (relative humidity = RH = 57%). The dried SC samples were processed by MM as follows: they were melt-mixed (8 min, 110°C, 100 rpm) in micro-extruder (μ-processing DSM; Netherlands) and then compression molded (SC + MM samples) at 120°C (4 min, 50 kN + 2 min, 150 kN) by hydraulic press (Fontijne Grotnes, Netherlands). As the properties of TPS samples are very sensitive to the humidity, all samples were stored in a desiccator with saturated solution of sodium bromide (RH = 57%); the samples were closed in the desiccator immediately after the preparation and kept there in between all experiments.

TABLE 1 | List of prepared TPS-based composites.

Sample	S [wt.%]	G [wt.%]	TiO_2 [wt.%]	TiNT [wt.%]
TPS(w)	70.0	30.0	–	–
TPS (w)/TiO_2 (3%)	68.0	29.0	3	–
TPS(w)/TiO_2 (6%)	65.8	28.2	6	–
TPS(w)/TiNT (3%)	68.0	29.0	–	3
TPS(t)	70.0	30.0	–	–
TPS(t)/TiO_2 (3%)	68.0	29.0	3	–
TPS(t)/TiO_2 (6%)	65.8	28.2	6	–
TPS(t)/TiNT (3%)	68.0	29.0	–	3

(w), wheat starch; (t), tapioca starch.
All samples contained residual water after processing by solution casting and melt mixing (ca 5%).

Characterization of TPS /TiX Composites

Light Microscopy

The overall homogeneity of the filler dispersion at lower magnifications was checked with a light microscope Nikon Eclipse 80i (Nikon, Japan) equipped with a digital camera ProgRes CT3 (Jenoptik, Germany). Thin sections (∼40 μm) were cut with a rotary microtome RM 2155 (Leica, Germany), put in oil between the support and cover glasses and observed with transmitted light using the bright field imaging.

Scanning Electron Microscopy

The morphology of the TPS matrix and the TPS/TiX composites at higher magnifications was visualized with a high resolution field-emission gun scanning electron microscope (SEM; microscope MAIA3, Tescan, Czech Republic) using a secondary electron imaging (SEM/SE) and a backscattered electron imaging (SEM/BSE) at 10 kV. The homogeneity of the TPS matrix was visualized as follows: the samples were broken in liquid nitrogen (below the glass transition temperature of TPS), the specimens were fixed on a metallic support using silver paste (Leitsilber G302, Christine Groepl, Austria), the fracture surfaces were covered with a thin Pt layer (∼8 nm; vacuum sputter coater, SCD 050, Balzers, Liechtenstein) and observed with a SE detector, which yielded mostly topographic contrast. The dispersion of TiX fillers in composites was observed using BSE detector that yielded mostly material contrast. The samples for BSE imaging were covered just by thin carbon layer (∼5 nm; vacuum evaporation device JEE-4C; JEOL, Japan) in order to maintain high compositional contrast between the TiX filler and the TPS matrix.

Transmission Electron Microscopy

The dispersion of the individual TiO_2 nanoparticles in the TPS matrix at the highest magnifications was visualized with a transmission electron microscope (TEM; microscope Tecnai G2 Spirit, FEI, Czech Republic). The ultrathin sections were prepared by a dry cryo-ultramicrotomy (ultramicrotome Ultracut EM UC7; Leica, Austria; cutting conditions: knife temperature = −50°C, sample temperature = −80°C, and dry cutting = sections collected directly from the knife face, without using water trough, onto a standard carbon-coated TEM grids).

The dried samples were observed in the TEM microscope at 120 kV using bright field imaging.

Wide-Angle X-Ray Diffraction (WAXD)

Diffraction patterns were obtained using a high resolution diffractometer Explorer (GNR Analytical Instruments, Italy). The instrument is equipped with a one-dimensional silicon strip detector Mythen 1K (Dectris, Switzerland). Samples were measured in a reflection mode. The radiation CuKα (wavelength $\lambda = 1.54$ Å) monochromatized with Ni foil (β filter) was used for diffraction. The measurement was done in range $2\Theta =$ 10–40° with step 0.1°. The exposure time at each step was 10 s. The peak deconvolution procedure was made using Fityk software (Wojdyr, 2010).

Attenuated Total Reflectance Infrared Spectroscopy

The infrared spectra of TPS and TPS/TiX composites were acquired using a Golden Gate single reflection attenuated total reflectance cell (ATR; Specac, Ltd., Orpington, Kent, UK) using a Fourier-transform infrared spectrometer (FTIR) Thermo Nicolet Nexus 870 (Thermo Fisher Scientific Inc., Waltham, Massachusetts, USA) purged with dry air. The spectrometer was equipped with a liquid nitrogen cooled MCT (mercury cadmium telluride) detector, and the ATR cell employed a diamond internal reflection element. ATR FTIR spectra were recorded with a resolution of 4 cm^{-1}; 256 scans were averaged per spectrum. After the subtraction of the spectrum of the ambient atmosphere, the baselines were corrected (linear base-line correction) and an advanced ATR correction was applied (the correction is defined and recommended within the control FTIR software OMNIC).

Rheometry

The rheological properties of the TPS matrices and the TPS/TiX composites were studied in oscillatory shear flow using a Physica MCR 501 rheometer (Anton Paar GmbH, Austria). A special anti-slipping parallel-plate geometry of 25 mm diameter plates was used. The sample thickness was around 1 mm. The experiments were performed at 120°C in the linear viscoelastic range (LVE range), confirmed from a strain sweep tests at the frequency of 1 Hz. Dynamic frequency sweeps test were carried out over the frequency range of 10^{-1}-10^{2} rad/s at a strain of 0.02%.

Dynamic Mechanical Analysis

The mechanical properties of the TPS/TiX composites were tested by a dynamic-mechanical analysis (DMA). The linear viscoelastic characteristics—the absolute value of complex modulus $|G^*|$, storage modulus *G'*, loss modulus *G"*, and loss factor tan(δ)—were measured in the rectangular torsion using a Physica MCR 501 rheometer (Anton Paar GmbH, Austria). The strain amplitude sweep tests (at −90°C and + 120°C) were conducted at the frequency 1 Hz in order to determine the linear viscoelastic range of all TPS/TiX composites. The temperature sweep measurements were carried out in the temperature range −90°C to 120°C (with heating rate 3°C /min), at a strain of 0.05% (in the linear viscoelastic range), and frequency 1 Hz.

Thermal Gravimetric Analysis

The thermal gravimetric analysis (TGA) of TPS/TiX samples (4–7 mg) was performed on a Perkin Elmer Pyris 1 TGA in the temperature range from 30 to 600°C at a rate of 10°C/min. The nitrogen purge gas flow rate was fixed at 25 ml/min of nitrogen.

RESULTS AND DISCUSSION

Morphology of TPS Composites

All TPS/TiO_2 and TPS/TiNT composites (**Table 1**) after the solution casting (SC) and its combination with the melt mixing (SC + MM) were visualized by LM (**Figure 1**). Lower magnification LM micrographs evidenced that the agglomerates of TiO_2 particles formed after SC (**Figures 1A–F**) were destroyed after SC + MM (**Figures 1G–L**). The LM micrographs also proved that the TPS(t)/TiX composites (**Figures 1D–F**, **J–L**) had a better TiX particles dispersion than the TPS(w)/TiX composites (**Figures 1A–C,G–I**), both after SC and after SC + MM. Both wheat and tapioca TPS/TiNT composites contained large agglomerates of TiNT after SC and also after SC+MM, but TPS(t)/TiNT composites exhibited less coarse morphology with slightly smaller agglomerates. The large agglomerates of TiNT dominated the morphology of all TPS/TiNT composites, being clearly visible even at low-magnification LM micrographs. Therefore, a morphological study of TPS/TiNT composites at higher magnifications was not necessary. In contrast, the fine morphology of TPS/TiO_2 composites was studied in more detail using SEM and TEM. Higher magnification SEM (**Figure 2**) micrographs showed that the TiO_2 particles tended to envelope plasticized, but not-fully-merged starch granules after SC (**Figures 2A,C**), while the following MM step resulted in complete merging of starch granules and very homogeneous distribution of TiO_2 nanoparticles (**Figures 2B,D**). The highest magnification TEM micrographs confirmed that tapioca TPS/TiO_2 composites had better dispersion of the fillers in nanoscale (**Figure 3**), which was not evident from SEM micrographs due to their limited resolution (higher magnification in SEM was impossible due to electron beam damage of the specimens). All three microscopic methods indicated that: (i) the two-step preparation (SC + MM) was necessary to get fully plasticized starch with homogeneous filler dispersion, which was in agreement with our previous study (Ostafinska et al., 2017) and that (ii) the two-step SC + MM method was quite universal, applicable not only to one particular wheat starch matrix, but also to different starch types.

XRD and IR Characterization

The structural changes of native wheat starch during its plasticization by our two-step preparation method (SC + MM) were studied in detail in our previous paper (Ostafinska et al., 2017). The paper dealt with wheat starch composites with low filler concentrations (up to 3%). In this paper we added characterization of the composites with different TPS matrices (tapioca starch and wheat starch from a different supplier) and the higher concentration of the fillers (up to 6 wt.%).

The XRD patterns of the samples containing wheat starch are present on **Figure 4A** and the tapioca-based samples are shown

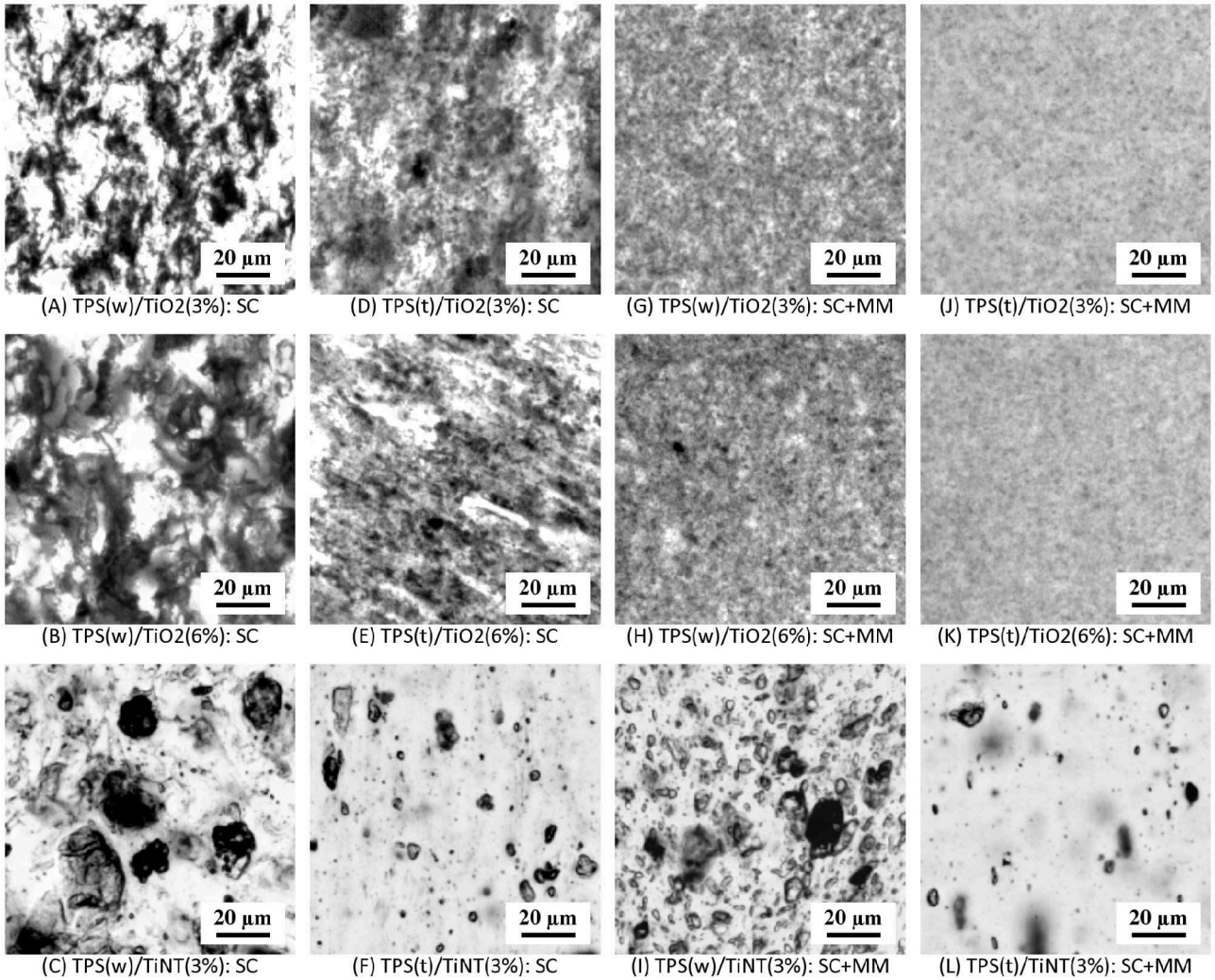

FIGURE 1 | LM micrographs showing the dispersion of filler in TPS/TiX composites: **(A–C)** wheat starch composites after solution casting, **(D–F)** tapioca starch composites after solution casting, **(G–I)** wheat starch composites after solution casting and melt-mixing, and **(J–L)** tapioca starch composites after solution casting and melt mixing.

on **Figure 4B**. Almost identical diffraction peaks were observed in native wheat and native tapioca starches. Those characteristic diffraction peaks of native starches (Zeng et al., 2011) disappeared in the plasticized samples, which proved the destruction of the original crystalline structure. Evidently, a retrogradation was taking place similarly to what was shown by Ostafinska et al. (2017). Two strong peaks at $2\Theta = 12.9^\circ$ and 19.8° were visible in the case of wheat starch [TPS(w)], indicating molecule rearrangement into V_H crystal lattice (van Soest et al., 1996). For the plasticized tapioca starch [TPS(t)] both peaks were present as well, but their intensity was lower. We have not observed presence of the other two known processing-induced crystal structures of TPS (V_A and E_H), which were described elsewhere (van Soest et al., 1996). For the samples with TiO_2, intense sharp peak at $2\Theta = 25.3^\circ$ corresponded to (101) diffraction of the TiO_2 anatase phase. The peak height was proportional to the content of TiO_2. For the samples with TiNT, no specific peaks corresponding to titanate nanotubes were detected, probably due to their low intensity; this was in agreement with analogous systems studied in our previous work (Ostafinska et al., 2017). Nevertheless, both composites with titanate nanotubes exhibited low-intensity broad residual crystallinity shoulder at 17.6°.

The ATR FTIR spectra of pure plasticized wheat starch [TPS(w)] and tapioca starch [TPS(t)] were not significantly different. Similarly, the spectra of the composites with TiX did not show significant changes compared to the original pure starch. The only region indicating some structural changes of TPS matrix is shown in **Figure 5**. In order to emphasize the subtle changes in the spectra of the composites, we subtracted the spectrum of pure plasticized starch from the spectrum of the composite with such a subtraction factor that no counter-peaks appeared in the resulting difference spectrum

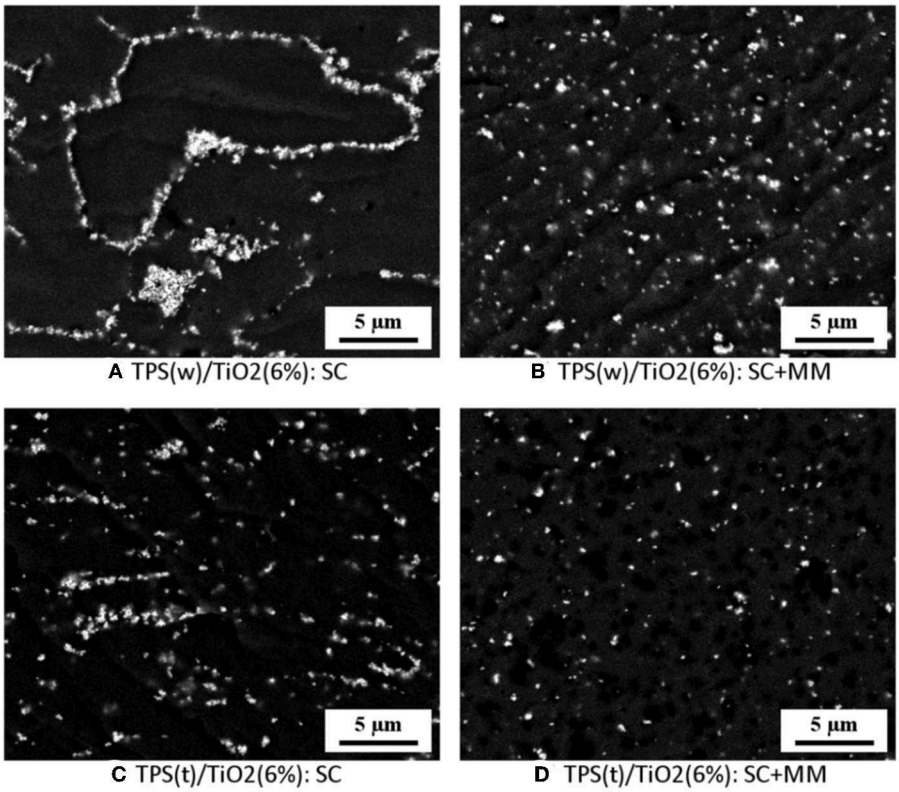

FIGURE 2 | SEM/BSE micrographs showing TPS/TiO_2(6%) composites: **(A,B)** wheat starch composite TPS(w)/TiO_2 (6%) and **(C,D)** tapioca starch composite TPS(t)/TiO_2 (6%); left column **(A,C)** shows composites after solution casting and right column **(B,D)** shows composites after solution casting and melt mixing.

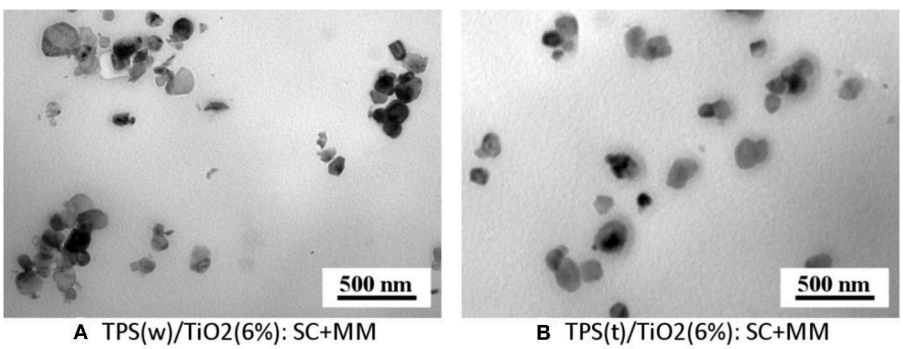

FIGURE 3 | TEM micrographs showing selected TPS/TiO_2 (6%) composites after solution casting and melt mixing: **(A)** wheat starch composite TPS(w)/TiO_2 (6%) and **(B)** tapioca starch composite TPS(t)/TiO_2 (6%).

(**Figure 5**). Relevant changes were detected in the region 1,100–950 cm^{-1} with bands corresponding to C-O, C-C stretching, and C-O-H bending vibrations. The bands at 1,045 and 1,000 cm^{-1} are assigned to crystalline and the band at 1,025 cm^{-1} to amorphous phase of starch. In the spectra of tapioca [TPS(t)/TiO_2] composites, the decrease in band intensity at 1,045 cm^{-1} indicated a decrease in crystallinity and a shift of the amorphous band from 1,025 cm^{-1} to higher wavenumbers suggested a strong interaction of the TiO_2 particles with the amorphous part of TPS(t) matrix. It can be seen in the spectra that the addition of TiNT resulted in a much stronger interaction and matrix destruction which is supported by a new band at 1,057 cm^{-1} and a decrease of the band around 1,080 cm^{-1} (C-O-H bending). On the other hand, in wheat composites [TPS(w)/TiX], the interactions between TiX fillers and the matrix were negligible. The addition of TiO_2 seemed to increase the crystallinity of the composites, while TiNT had no clear effect on the composites.

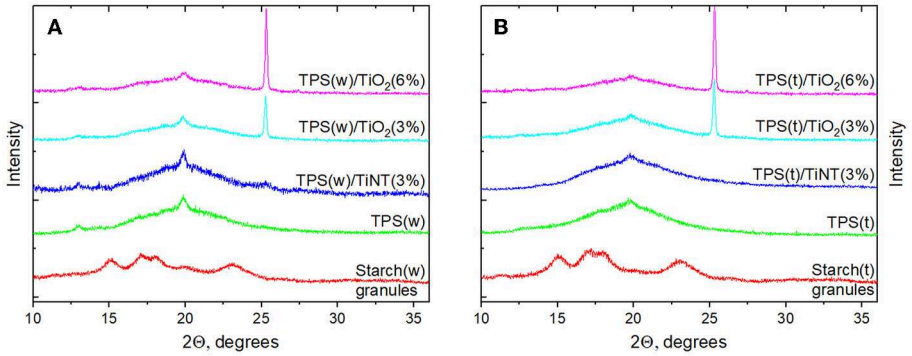

FIGURE 4 | X-ray diffraction patterns of wheat **(A)** and tapioca **(B)** TPS/TiX composites.

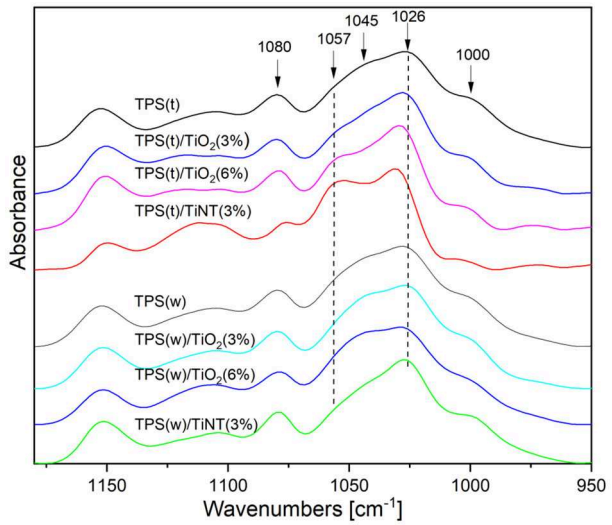

FIGURE 5 | IR spectra of plasticized tapioca and wheat starch and difference spectra of the TPS/TiX composites. From the spectra of all TPS/TiX composites, the spectra of the corresponding pure plasticized starches [TPS(t) or TPS(w)] were partially subtracted in order to emphasize difference peaks, as described in section XRD and IR characterization.

Rheological Properties

The rheological properties of the TPS/TiX composites in the oscillatory shear at 120°C are shown in **Figures 6**, **7**. The logarithmic dependence of the complex viscosity ($|\eta^*|$) on angular frequency (ω) for the wheat composites [TPS(w)/TiX] showed a linear decrease almost in the whole range 0.1–100 rad/s, whereas for the tapioca composites [TPS(t)/TiX] it showed the significant curvature down for the lowest ω (region ω = 0.1–0.4 rad/s; **Figure 6**). The values of the complex viscosity ($|\eta^*|$) of the TPS(t)/TiO_2 composites were higher in the whole range of frequencies than that of all TPS(w)/TiX composites. Influence of 3 wt.% TiX particles on the complex viscosity of wheat TPS was low, which accorded with our previous work (Ostafinska et al., 2017). The TPS(t)/TiX composites showed different rheological behavior. Firstly, the addition of TiO_2 to the TPS(t) matrix increased the complex viscosity with a slight further increase for the composites with 3 and 6 wt.% of TiO_2 particles. Secondly, the addition of TiNT to the TPS(t) matrix decreased the complex viscosity. This was in agreement with the LM, SEM, TEM, and IR results described above: (i) all microscopic methods confirmed the finer dispersion of the TiO_2 particles in TPS(t) composites in comparison with the TPS(w) composites (**Figures 1**–**3**) and (ii) the IR spectroscopy results suggested the stronger interactions of the TiO_2 particles with the TPS(t) matrix in comparison with the TPS(w) matrix (**Figure 5** and its discussion in the previous section). Therefore, the very homogeneously dispersed TiO_2 particles, which strongly interacted with the TPS(t) matrix, formed a relatively strong physical network and *increased* the $|\eta^*|$ values of the TPS(t)/TiO_2 composites. Moreover, the IR spectra suggested that TiNT partially destroyed the internal structure of the TPS(t) matrix, which *decreased* the $|\eta^*|$ values of TPS(t)/TiNT composites. Finally, the IR spectra of TPS(w) composites indicated negligible interactions of all TiX fillers with the TPS(w) matrix, which resulted in just a small increase in the viscosity of TPS(w)/TiX composites, corresponding to the fact that we added a small amount of the hard inorganic filler into the soft polymer matrix.

The storage modulus (G') was larger than the loss modulus (G'') in the whole range of angular frequencies for both wheat and tapioca TPS/TiX composites (**Figure 7**), which is typical of crosslinked and high-molecular weight polymers. In the case of TPS(w) and TPS(w)/TiX composites, G' increased almost linearly for $\omega > 0.4$ rad/s in logarithmic plot. In the case of the TPS(t) and TPS(t)/TiX composites, the almost-linear growth of G' started at higher frequencies [for TPS(t) at $\omega > 30$ rad/s, for TPS(t)/TiNT at $\omega > 40$ rad/s, and for TPS(t)/TiO_2 at $\omega > 15$ rad/s]. The curving down of the G' value with the decreasing ω is typical of non-crosslinked polymers (Mezger, 2014). Surprisingly enough, this effect was observed for the higher-viscosity TPS(t) composites and not for the lower-viscosity TPS(w) composites. The higher values of G', G'', and $|G^*|$ for TPS(t)/TiO_2 composites in comparison with the TPS(t) matrix (**Figures 7**, **8**) confirmed our assumption that the TiO_2 nanoparticles in TPS(t) matrix formed a physical network due to their almost ideal dispersion.

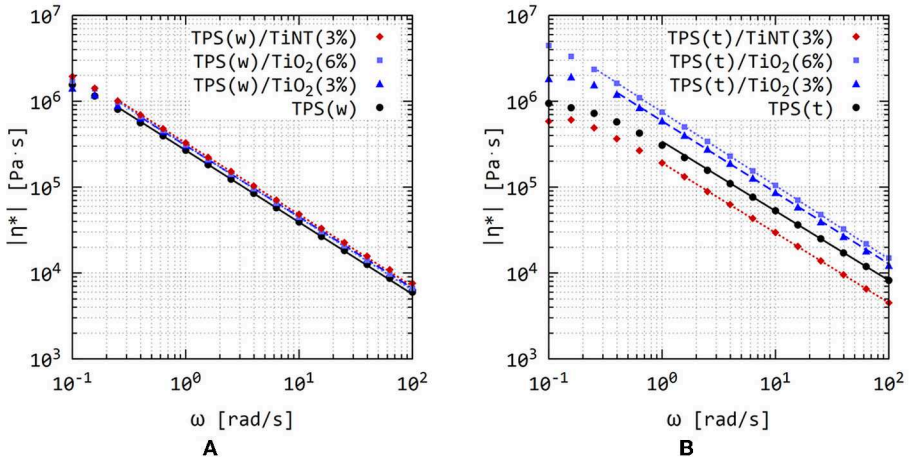

FIGURE 6 | The absolute values of complex viscosities of wheat **(A)** and tapioca **(B)** TPS/TiX composites at 120°C and strain 0.02%: the comparison of the frequency sweeps and their fitting with power-law model (dotted lines; description of the model in Ostafinska et al. (2017).

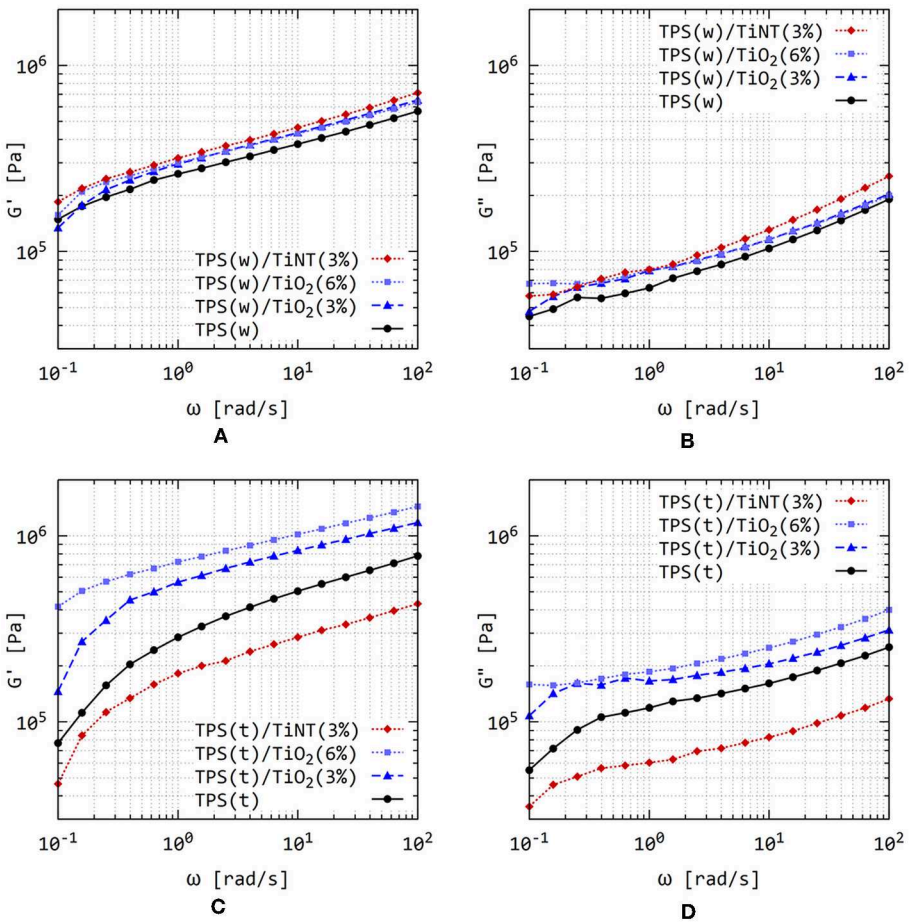

FIGURE 7 | The values of storage modulus (*G'*) **(A,C)** and loss modulus (*G''*) **(B,D)** of wheat **(A,B)** and tapioca **(C,D)** TPS/TiX composites at 120°C and strain 0.02%.

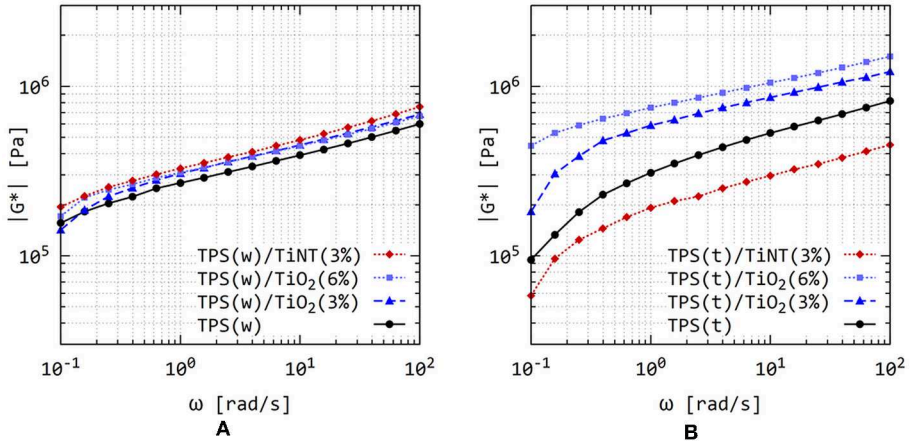

FIGURE 8 | The absolute values of complex modulus (|G*|) of wheat **(A)** and tapioca **(B)** TPS/TiX composites at 120°C and strain 0.02%.

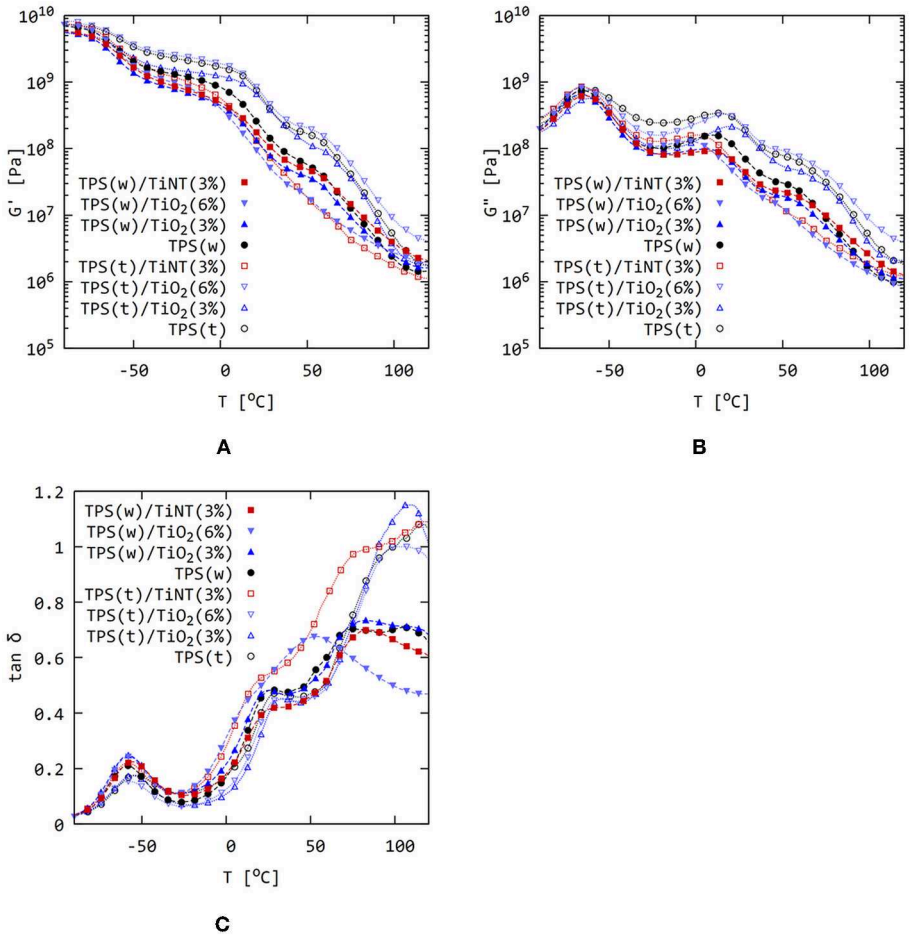

FIGURE 9 | Dynamic mechanical thermal analysis of wheat (w) and tapioca (t) TPS/TiX composites at angular frequency 1 Hz and strain 0.05%: **(A)** storage modulus (*G′*), **(B)** loss modulus (*G″*), and **(C)** damping factor [tan (δ)].

The lower values G', G'', and $|G^*|$ for TPS(t)/TiNT composites in comparison with neat TPS(t) can be explained as follows: Basic features of TPS in flow are typical of thermoplastic materials but the structure of TPS is more complex in comparison with simple polymer melts. We even detected two glass transition temperatures (see section Thermomechanical Properties below) related to the two-phase structure of TPS. Moreover, all phases of TPS have their own complex supramolecular structures due to multiple hydrogen bond-based interactions. The supramolecular structures obviously affect rheological properties (rheological response of ordered structures is similar to temporary crosslinks). The assumption that TiNT partially destroyed the original structure of TPS(t) matrix is the most probable explanation of observed decrease in viscosity and modulus. Further changes of supramolecular structure could occur due to possible TiNT-induced scissions of amylose and amylopectin chains. For all prepared composites, the G' and G'' were more-or-less parallel lines and the absolute value of complex moduli $|G^*|$ (**Figure 8**) were almost as high as G', which was in agreement with solid-like, crosslinked structure of TPS-based materials (Mezger, 2014). It should be mentioned that the solid-like behavior of TPS and its composites is not a consequence of chemical networks but of long-living entanglements between extremely long starch chains and/or aggregates kept by non-covalent interactions. Similar behavior of TPS matrix was observed in our previous study dealing with TPS(w)/TiX composites with lower concentration of fillers (Ostafinska et al., 2017). Complex rheological behavior of TPS matrices, including two glass transition temperatures, was observed by other research groups (Viguie et al., 2007; Sessini et al., 2017, 2018); this is discussed also in the following section dealing with DMTA results. Strong hydrogen bond interactions between TPS matrix and TiO_2 nanoparticles were observed also in the recent study of (Xiong et al., 2019).

Thermomechanical Properties

The dynamic mechanical thermal analysis (DMTA) of wheat and tapioca TPS/TiX composites was carried out in order to characterize the difference between the two starch types and the influence of the TiX particles on the phase changes of the TPS-based composites (**Figure 9**). The TPS(t) matrix and TPS(t)/TiO_2 composites were stiffer than the corresponding TPS(w) samples [G' of TPS(t) samples > G' of TPS(w) samples]. As expected, the G'-curves of all systems decreased with the increasing temperature (**Figure 9A**). G' was higher than G'' for most studied systems in the whole range of temperatures, which confirmed the gel-like structure and the physical stability of all systems (Ross-Murphy, 1995). In the case of TPS(t)/TiO_2 composites, the G' became equal to G'' at 90°C and then G'' became slightly higher than G'. This indicated a dominating viscous behavior of TPS(t) composites at elevated temperatures. The TPS(t)/TiNT composite showed low G' in the whole range of temperatures. Moreover, the TPS(t)/TiNT composites exhibited $G' = G''$ at 73°C. These facts supported our assumption from IR and rheological measurements (sections **XRD and IR Characterization** and Rheological Properties) that the original structure TPS(t) was partially destroyed due to the addition of TiNT. The loss modulus (G'') and the damping factor [tan(δ)] curves (**Figures 9B,C**) showed two local maxima which corresponded to the two glass transition temperatures (T_g) of TPS matrices: "glycerol-rich phase" (below 0°C) and "amylopectin-rich phase" (above 0°C) as described elsewhere (Viguie et al., 2007; Sessini et al., 2017, 2018). **Figures 9B,C** show that the T_g value of the "glycerol-rich phase" was the same for both tapioca and wheat TPS and their composites, whereas the T_g values of "amylopectin-rich phase" differed [T_g of TPS(w) < T_g of TPS(t)]. This was attributed to different chain domains of the high-molecular weight branched amylopectin molecules in particular starches. Namely, this indicated a decreased mobility of "starch-rich phase" in TPS(t) systems in comparison to TPS(w) (Viguie et al., 2007; Sessini et al., 2018).

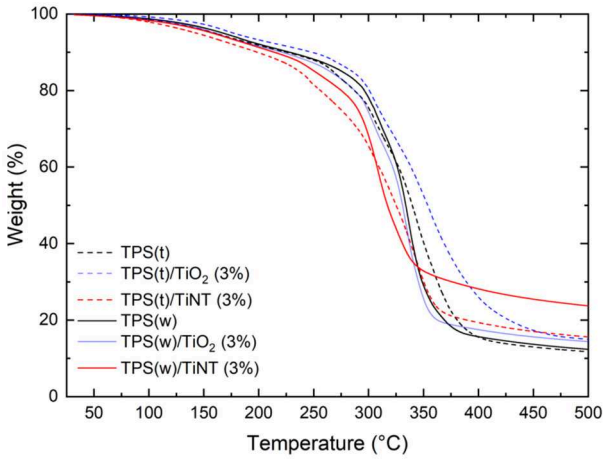

FIGURE 10 | TGA curves of TPS/TiX composites.

TABLE 2 | TGA Results: Weight losses and weight residue (wt.%) of starch samples during thermal degradation under nitrogen atmosphere and heating rate 10°C/min.

	Weight loss between 30 and 120°C (%)	Weight loss between 120 and 400°C (%)	Weight residue at 500°C (%)
TPS (t)	2.5	83	12
TPS (t)/TiO_2 (3%)	2.0	73	15
TPS (t)/TiNT (3%)	3.0	78	16
TPS (w)	2.5	83	12
TPS (w)/TiO_2 (3%)	2.5	81	14
TPS (w)/TiNT (3%)	2.5	70	24

(w), wheat starch; (t), tapioca starch.

Thermal Stability

Figure 10 shows the thermal stability of the TPS(t) and TPS(w) composites. **Table 2** summarizes selected TGA parameters. The first step of thermal degradation between 30 and 120°C was connected with the release of absorbed water. The TGA curves suggested that all systems contained similar amount of water and that they were quite stable until ∼250°C. The important exception was the TPS(t)/TiNT composite, which started to

degrade around 200°C. Also the TPS(w)/TiNT composite exhibited slightly lower thermal stability in comparison with the other samples. The second stage of thermal degradation was pyrolysis of starch and glycerol. The lower thermal stability of the TPS(t)/TiNT and TPS(w)/TiNT composites during the second stage of thermal degradation might indicate partial destruction of the TPS matrix structure. At temperatures above 400°C under nitrogen atmosphere, carbon black started to form. This was the reason of quite high weight residue at 500°C, which was approximately the same for all samples.

CONCLUSIONS

This paper was focused on the comparison of wheat and tapioca thermoplastic starches (TPS) and their composites with TiO_2-based nanoparticles (isometric TiO_2 nanoparticles and high aspect ratio TiNT nanotubes). The TPS composites were prepared by our recently developed two-step method that combines a solution casting and melt-mixing (SC + MM).

Main conclusions of our study can be summarized as follows: (i) The SC + MM procedure can be considered as the universal method for preparation of TPS composites with very homogeneous dispersion of the filler, regardless of the starch source and type. (ii) The type of TPS matrix (wheat or tapioca) has a significant impact on the properties of the final composite. (iii) The isometric TiO_2 nanoparticles exhibited very good filler dispersion in both TPS(w) and TPS(t) matrices, while TiNT nanotubes tended to form micrometer-sized agglomerates.

For all studied systems, the tapioca TPS [TPS(t)] composites showed somewhat better dispersion of the filler (as proved by three independent microscopic techniques—LM, SEM, and TEM), stronger interactions of the filler with the matrix (as indicated by IR) and, consequently, a higher impact of the filler on the final properties (as documented by the rheological and thermomechanical measurements). In the TPS(t)/TiO_2 composites, the dominating effect was the formation of the physical network of the well-dispersed filler particles, resulting in a significant increase in the final value of the complex viscosity, $|\eta^*|$. In the TPS(t)/TiNT composites, the dominating effect was the partial destruction of the TPS matrix, resulting in a decrease in $|\eta^*|$. In wheat TPS [TPS(w)] composites, all matrix-filler interactions were weak and so all TPS(w)/TiO_2 and TPS(w)/TiNT composites exhibited just a slight increase in $|\eta^*|$ due to the fact that we added a stiff inorganic filler into a soft polymer matrix. The above-described complex viscosity changes correlated with other rheological and thermomechanical properties.

DATA AVAILABILITY STATEMENT

The datasets generated for this study are available on request to the corresponding author.

AUTHOR CONTRIBUTIONS

MS, IF, and AU designed the study. AU with the help of SK prepared the TPS and TPS composites by solution casting and melt mixing, and characterized the samples by light and electron microscopy. MN with AU performed and evaluated rheology and DMTA measurements. JD and AZ measured and processed IR and XRD data, respectively. JK carried out TGA measurements and helped with their interpretation. MS with IF made the final data interpretation, with an important contribution of JD. AU prepared draft of the manuscript, which was finalized by MS.

FUNDING

Financial support through grant NV15-31269A (MH CR) is gratefully acknowledged. Electron microscopy at the Institute of Macromolecular Chemistry was supported by projects TE01020118, TN01000008 (Technology Agency of the CR), and POLYMAT LO1507 (Ministry of Education, Youth and Sports of the CR, program NPU I).

REFERENCES

Ajiya, D. A., Jikan, S. S., Talip, B. H. A., Badarulzaman, N. A., Matias-Peralta, H. M., Derawi, D., et al. (2017). The influence of glycerol on mechanical, thermal and morphological properties of thermoplastic tapioca starch film. *J. Sci. Technol.* 9, 24–29. Retrieved from: https://publisher.uthm.edu.my/ojs/index.php/JST/article/view/2054

Altskar, A., Andersson, R., Boldizar, A., Koch, K., Stading, M., Rigdahl, M., et al. (2008). Some effects of processing on the molecular structure and morphology of thermoplastic starch. *Carbohyd. Polym.* 71, 591–597. doi: 10.1016/j.carbpol.2007.07.003

Ao, Z., and Jane, J. (2007). Characterization and modeling of the A- and B-granule starches of wheat, triticale, and barley. *Carbohyd. Polym.* 67, 46–55. doi: 10.1016/j.carbpol.2006.04.013

Bergel, B. F., Machado da Luz, L., and Santana, R. M. C. (2017). Comparative study of the influence of chitosan as coating of thermoplastic starch foam from potato, cassava and corn starch. *Prog. Org. Coatings* 106, 27–32. doi: 10.1016/j.porgcoat.2017.02.010

Bertolini, A. (2010). *Starches: Characterization, Properties, and Applications*. Boca Raton, FL: CRC Press; Taylor & Francis Group.

Biliaderis, C. G. (2009). "Structural transitions and related physical properties of starch," in *Starch. Chemistry and Technology. A Volume in Food Science and Technology, 3rd Edn.*, ed J. BeMiller, and R. Whistler (Burlington; London; San Diego, CA; New York, NY: Academic Press), 293–372.

Breuninger, W. F., Piyachomkwan, K., and Sriroth, K. (2009). "Tapioca/cassava starch: production and use," in *Starch. Chemistry and Technology. A Volume in Food Science and Technology, 3rd Edn.,* ed J. BeMiller, and R. Whistler (Burlington; London; San Diego, CA; New York, NY: Academic Press), 541–568.

Campos, A., Sena Neto, A. R., Rodrigues, V. B., Luchesi, B. R., Mattoso, L. H. C., and Marconcini, J. M. (2018). Effect of raw and chemically treated oil palm mesocarp fibers on thermoplastic cassava starch properties. *Ind. Crops Prod.* 124, 149–154. doi: 10.1016/j.indcrop.2018.07.075

Campos, A., Senta Neto, A. R., Rodrigues, V. B., Luchesi, B. R., Moreira, F. K. V., Correa, A. C., et al. (2017). Bionanocomposites produced from cassava starch and oil palm mesocarp cellulose nanowhiskers. *Carbohyd. Polym.* 175, 330–336. doi: 10.1016/j.carbpol.2017.07.080

Campos-Requena, V. H., Rivas, B. L., Perez, M. A., Figueroa, C. R., Figueroa, N. E., and Sanfuentes, E. A. (2017). Thermoplastic starch/clay nanocomposites loaded with essential oil consituents as packaging for strawberries – *in vivo*

entimicrobial synergy over *Botrytis cinerea*. *Postharvest Biol. Technol.* 129, 29–36. doi: 10.1016/j.postharvbio.2017.03.005

Chang, Y. P., Karim, A. A., and Seow, C. C. (2006). Interactive plasticizing–antiplasticizing effects of water and glycerol on the tensile properties of tapioca starch films. *Food Hydrocolloids* 20, 1–8. doi: 10.1016/j.foodhyd.2005.02.004

Dai, H., Chang, P., Yu, J., and Ma, X. (2008). N,N-Bis(2-hydroxyethyl)formamide as a new plasticizer for thermoplastic starch. *Starch/Starke* 60, 676–684. doi: 10.1002/star.200800017

Garcia, N. L., Ribba, L., Dufresne, A., Aranguren, M. I., and Goyanes, S. (2009). Physico-mechanical properties of biodegradable starch nanocomposites. *Macromol. Mater. Eng.* 294, 169–177. doi: 10.1002/mame.200800271

Genovese, L., Dominici, F., Gigli, M., Armentano, I., Lotti, N., Fortunati, E., et al. (2018). Processing, thermo-mechanical characterization and gas permeability of thermoplastic starch/poly(butylene trans-1,4-cyclohexanedicarboxylate) blends. *Polym. Degrad. Stability* 157, 100–107. doi: 10.1016/j.polymdegradstab.2018.10.004

Ghavimi, S. A. A., Ebrahimzadeh, M. H., Shokrgozar, M. A., Solati-Hashjin, M., and Osman, N. A. A. (2015). Effect of starch content on the biodegradation of polycaprolactone/starch composite for fabricating in situ pore-forming scaffolds. *Polym. Test.* 43, 94–102. doi: 10.1016/j.polymertesting.2015.02.012

Gonzalez-Seligra, P., Guz, L., Ochoa-Yepes, O., Goyanes, S., and Fama, L. (2017). Influence of extrusion process conditions on starch film morphology. *LWT Food Sci. Technol.* 84, 520–528. doi: 10.1016/j.lwt.2017.06.027

Guz, L., Candal, R., and Goyanes, S. (2017). Size effect of ZnO nanorods on physicochemical properties ofplasticized starch composites. *Carbohyd. Polym.* 157, 1611–1619. doi: 10.1016/j.carbpol.2016.11.041

Jane, J.-L. (2009). "Structural features in starch granules II," in *Starch. Chemistry and Technology. A Volume in Food Science and Technology, 3rd Edn.*, eds J. BeMiller, and R. Whistler (Burlington; London; San Diego, CA; New York, NY: Academic Press), 193–236.

Javanbakht, S., and Namazi, H. (2017). Solid state photoluminescence thermoplastic starch film containing graphene quantum dots. *Carbohyd. Polym.* 176, 220–226. doi: 10.1016/j.carbpol.2017.08.080

Kargarzadeh, H., Johar, N., and Ahmad, I. (2017). Starch biocomposite film reinforced by multiscale rice husk fiber. *Composit. Sci. Technol.* 151, 147–155. doi: 10.1016/j.compscitech.2017.08.018

Kelnar, I., Kapralkova, L., Brozova, L., Hromadkova, J., and Kotek, J. (2013). Effect of chitosan on the behaviour of the wheat B-starch nanocomposite. *Ind. Crops Prod.* 46, 186–190. doi: 10.1016/j.indcrop.2013.01.030

Kralova, D., Slouf, M., Klementova, M., Kuzel, R., and Kelnar, I. (2010). Preparation of gramquantities of high-quality titanate nanotubes and their composites withpolyamide 6. *Mater. Chem. Phys.* 124, 652–657. doi: 10.1016/j.matchemphys.2010.07.029

Kuswandi, B. (2017). Environmental friendly food nano-packaging. *Environ. Chem. Lett.* 15, 205–221. doi: 10.1007/s10311-017-0613-7

Liu, G., Gu, Z., Hong, Y., Cheng, L., and Li, C. (2017b). Electrospun starch nanofibres: recent advances, challenges, and strategies for potential pharmaceutical applications. *J. Contr. Release* 252, 95–107. doi: 10.1016/j.jconrel.2017.03.016

Liu, P., Yu, L., Wang, Z., Li, D., Chen, L., and Li, X. (2010). Glass transition temperature of starches with different amylose/amylopectin ratios. *J. Cereal Sci.* 51, 388–391. doi: 10.1016/j.jcs.2010.02.007

Liu, S., Li, X., Chen, L., Li, L., Li, B., and Zhu, J. (2017a). Understanding physicochemical properties changes from multi-scale structures of starch/CNT nanocomposite films. *Int. J. Biol. Macromol.* 104, 1330–1337. doi: 10.1016/j.ijbiomac.2017.05.174

Liu, X., Wang, Y., Yu, L., Tong, Z., Chen, L., Liu, H., et al. (2013). Thermal degradation and stability of starch under different processing conditions. *Starch/Starke* 65, 48–60. doi: 10.1002/star.201200198

Liu, Y. X., Fan, L. L., Mo, X. Z., Yang, F., and Pang, J. Y. (2018). Effects of nanosilica on retrogradation properties and structures of thermoplastic cassava starch. *J. Appl. Polym. Sci.* 135:45687. doi: 10.1002/app.45687

Lopez-Cordoba, A., Medina-Jaramillo, C., Pineros-Hernandez, D., and Goyanes, S. (2017). Cassava starch films containing rosemary nanoparticles produced by solvent displacement method. *Food Hydrocolloids* 71, 26–34. doi: 10.1016/j.foodhyd.2017.04.028

Mahieu, A., Terrie, C., and Youssef, B. (2015). Thermoplastic starch films and thermoplastic starch/polycaprolactone blends with oxygen-scavenging properties: Influence of water content. *Ind. Crops Prod.* 72, 192–199. doi: 10.1016/j.indcrop.2014.11.037

Maningat, C. C., Seib, P. A., Bassi, S. D., Woo, K. S., and Lasater, G. D. (2009). "Wheat starch: production, properties, modification and uses," in *Starch. Chemistry and Technology. A Volume in Food Science and Technology, 3rd Edn.*, eds J. BeMiller, and R. Whistler, 441–510.

Mezger, T. G. (2014). *The Rheology Handbook, 4th Edn.* Hannover: Vincentz Network GmbH.

Oleyaei, S. A., Almasi, H., Ghanbarzadeh, B., and Moayedi, A. A. (2016a). Synergistic reinforcing effect of TiO_2 and montmorillonite on potato starch nanocomposite films: thermal, mechanical and barrier properties. *Carbohyd. Polym.* 152, 253–262. doi: 10.1016/j.carbpol.2016.07.040

Oleyaei, S. A., Zahedi, Y., Ghanbarzadeh, B., and Moayedi, A.A. (2016b). Modification of physicochemical and thermal properties of starch films by incorporation of TiO_2 nanoparticles. *Int. J. Biol. Macromol.* 89, 256–264. doi: 10.1016/j.ijbiomac.2016.04.078

Omotoso, M. A., Adeyefa, O.S., Animashaun, E. A., and Osibanjo, O. O. (2015). Biogradable starch film from cassava, corn, potato and yam. *Chem. Mater. Res.* 7, 15–24.

Ostafinska, A., Mikesova, J., Krejcikova, S., Nevoralova, M., Sturcova, A., Zhigunov, A., et al. (2017). Thermoplastic starch composites with TiO_2 particles: preparation, morphology, rheology and mechanical properties. *Int. J. Biol. Macromol.* 101, 273–282. doi: 10.1016/j.ijbiomac.2017.03.104

Perez, S., Baldwin, P. M., and Gallant, D. J. (2009). "Structural features of starch granules I," in *Starch. Chemistry and Technology. A Volume in Food Science and Technology, 3rd Edn.,* eds J. BeMiller, and R. Whistler, 149–192.

Pushpadass, H., Marx, D. B., and Hanna, M. A. (2008). Effects of extrusion temperature and plasticizers on the physical and functional properties of starch films. *Starch/Starke* 60, 527–538. doi: 10.1002/star.200800713

Razali, S. M., Yusoff, M., Ramle, S. F. M., Bhat, I. U. H., Iman, A. H. M., and Razali, A. M. H. (2016). The potential of donax grandis hypodermal fiber as a reinforcement in starch-based composite. *J. Polym. Mater.* 33, 677–684.

Ross-Murphy, S. B. (1995). Structure-property relationships in food biopolymer gels and solutions. *J. Rheol.* 39, 1451–1463. doi: 10.1122/1.550610

Saiah, R., Gatin, R., and Sreekumar, P. A. (2012). "Properties and biodegradation nature of thermoplastic starch," in *Thermoplastic Elastomers*, ed A. El-Sonbati (Rijeka: InTech), 57–78. Available online at: http://www.intechopen.com/books/thermoplastic-elastomers/properties-andbiodegradation-nature-of-thermoplastic-starch

Sarka, E., Krulis, Z., Kotek, J., Ruzek Korbarova, A., Bubnik, Z., and Ruzkova, M. (2011). Application of wheat B-starch in biodegradable plastic materials. *Czech J. Food Sci.* 29, 232–242. doi: 10.17221/292/2010-CJFS

Sarka, E., Krulis, Z., Kotek, J., Ruzek, L., Vorisek, K., Kolacek, J., et al. (2012). Composites containing acetylated wheat B-starch for agriculture applications. *Plant Soil Environ.* 58, 354–359. doi: 10.17221/287/2012-PSE

Schmitt, H., Guidez, A., Prashantha, K., Soulestin, J., Lacrampe, M. F., and Krawczak, P. (2015). Studies on the effect of storage time and plasticizers on the structuralvariations in thermoplastic starch. *Carbohyd. Polym.* 115, 364–372. doi: 10.1016/j.carbpol.2014.09.004

Sengottuvelan, A., Balasubramanian, P., Will, J., and Boccaccini, A. R. (2017). Bioactivation of titanium dioxide scaffolds by ALP-functionalization. *Bioact. Mater.* 2, 108–115. doi: 10.1016/j.bioactmat.2017.02.004

Sessini, V., Arriera, M. P., Fernandez-Torres, A., and Peponi, L. (2018). Humidity-activated shape memory effect on plasticized starch-based biomaterials. *Carbohyd. Polym.* 179, 93–99. doi: 10.1016/j.carbpol.2017.09.070

Sessini, V., Raques, J.-M., Lourdin, D., Maigret, J.-D., Kenny, J. M., Dubois, P., et al. (2017). Humidity-activated shape memory effects on thermoplastic starch/EVA blends and their compatibilized nanocomposites. *Macromol. Chem. Phys.* 218:1700388. doi: 10.1002/macp.201700388

Song, X., Zuo, G., and Chen, F. (2018). Effect of essential oil and surfactant on the physical and antimicrobialproperties of corn and wheat starch films. *Int. J. Biol. Macromol.* 107, 1302–1309. doi: 10.1016/j.ijbiomac.2017.09.114

Teixeira, E. M., Curvelo, A. A. S., Correa, A. C., Marconcini, J. M., Glenn, G. M., and Mattoso, L. H. C. (2012). Review. Properties of thermoplastic starch from cassava bagasse and cassava starch and their blends with poly (lactic acid). *Ind. Crops Prod.* 37, 61–68. doi: 10.1016/j.indcrop.2011.11.036

Teixeira, E. M., Pasquini, D., Curvelo, A. A. S., Corradini, E., Belgacem, M. N., and Dufresne, A. (2009). Cassava bagasse cellulose nanofibrils reinforced thermoplastic cassava starch. *Carbohyd. Polym.* 78, 422–431. doi: 10.1016/j.carbpol.2009.04.034

Valencia-Sullca, C., Vargas, M., Atares, L., and Chiralt, A. (2018). Thermoplastic cassava starch-chitosan bilayer films containing essential oils. *Food Hydrocolloids* 75, 107–115. doi: 10.1016/j.foodhyd.2017.09.008

van Soest, J. J. G., Hulleman, S. H. D., de Wit, D., and Vliegenthart, J. F. G. (1996). Crystallinity in starch bioplastics. *Ind. Crops Prod.* 5, 11–12. doi: 10.1016/0926-6690(95)00048-8

Viguie, J., Molina-Boisseau, S., and Dufresne, A. (2007). Processing and characterization of waxy maize starch films plasticized by sorbitol and reinforced with starch nanocrystals. *Macromol. Biosci.* 7, 1206–1216. doi: 10.1002/mabi.200700136

Visakh, P. M., Mathew, P. A., Oksman, K., and Thomas, S. (2012). "Starch-basedbionanocomposites: processing and properties," in *Polysaccharide Building Blocks: A Sustainable Approach to the Development of Renowable Biomaterials*, eds Y. Habibi, and L. A. Lucia (Hoboken, NJ: John Wiley & Sons, Inc.), 287–306.

Webster, J., Ergun, C., Doremus, R. H., Siegel, R. W., and Bizios, R. (2000). Enhanced functions of osteoblasts on nanophase ceramics. *Biomaterials* 21, 1803–1810. doi: 10.1016/S0142-9612(00)00075-2

Wojdyr, M. (2010). Fityk: a general-purpose peak fitting program. *J. Appl. Cryst.* 43, 1126–1128. doi: 10.1107/S0021889810030499

Xie, F., Pollet, E., Halley, P. J., and Averous, L. (2013). Starch-based nano-biocomposites. *Prog. Polym. Sci.* 38, 1590–1628. doi: 10.1016/j.progpolymsci.2013.05.002

Xiong, J. Y., Scheng, C. H., Wang, Q., and Guo, W. H. (2019). Toughened and water-resistant starch/TiO_2 bio-nanocomposites as an environment-friendly food packaging material. *Mater. Res. Exp.* 6:055045. doi: 10.1088/2053-1591/ab058b

Zeng, J., Li, G., Gao, H., and Ru, Z. (2011). Comparison of A and B starch granules from three wheat varieties. *Molecules* 16, 10570–10591. doi: 10.3390/molecules161210570

Zhu, F. (2015). Review. Composition, structure, physicochemical properties, and modifications of cassava starch. *Carbohyd. Polym.* 122, 456–480. doi: 10.1016/j.carbpol.2014.10.063

Zuo, G., Song, X., Chen, F., and Shen, Z. (2017). Physical and structural characterization of edible bilayer films made with zein and corn-wheat starch. *J. Saudi Soc. Agric. Sci.* 18, 324–331. doi: 10.1016/j.jssas.2017.09.005

Conflict of Interest: The authors declare that the research was conducted in the absence of any commercial or financial relationships that could be construed as a potential conflict of interest.